

PAPER · OPEN ACCESS

Optical characterizations of densely doped Tm³⁺:KYW crystals at low temperatures

To cite this article: Yisheng Lei et al 2024 J. Opt. 26 095401

View the article online for updates and enhancements.

You may also like

- Spectroscopy and microchip laser operation of Tm, Ho:KYW crystals with different Ho concentrations N V Gusakova, S V Kurilchik, A S Yasukevich et al.
- Optical shutters for a compact femtosecond Yb:KYW laser N N Rubtsova, A A Kovalyov, D V Ledovskikh et al.
- Phase-locking of octave-spanning optical frequency comb based on Kerr-lens modelocked Yb:KYW laser to reference laser Masatoshi Mitaki and Kazuhiko Sugiyama

J. Opt. 26 (2024) 095401 (7pp)

Optical characterizations of densely doped Tm³⁺:KYW crystals at low

Yisheng Lei®, Trevor Kling® and Mahdi Hosseini*®

Department of Electrical and Computer Engineering and Applied Physics Program, Northwestern University, Evanston, IL 60208, United States of America

E-mail: mh@northwestern.edu

Received 9 March 2024, revised 2 July 2024 Accepted for publication 8 July 2024 Published 17 July 2024

temperatures



https://doi.org/10.1088/2040-8986/ad6010

Abstract

We investigate the optical lifetime, decay characteristics, spectral linewidth and energy level properties of thulium ions doped in a $KY(WO_4)_2$ crystal at 4 K temperature. High doping concentration of thulium ions with inhomogeneous broadening allow us to study nonradiative behaviors, instantaneous spectral diffusion, and spectral power broadening in this solid-state material. The theoretical consideration of ion–ion interactions is shown to accurately characterize the absorption, decay and other spectral behaviors of Tm^{3+} ions. We observe more than ten-fold reduction in the decay time of 3H_4 state and about three-fold reduction in the spectral-hole lifetime as we approach the center of the inhomogeneous broadening, corresponding to higher optical densities.

Keywords: thulium, optical characterizations, KYW crystal

1. Introduction

Rare-earth-ion doped solids have wide applications in laser technologies [1–3] and quantum optical information, e.g. light storage [4, 5]. The choice of crystalline host is important when designing rare-earth crystals for different applications. One such host is potassium double tungstates, KX(WO₄)₂, where X = Gd, Y or Lu. KY(WO₄)₂ or KYW belongs to the monoclinic crystal system (space group: C2/c, Wyckoff position: 4e) with lattice constants a = 10.63 Å, b = 10.34 Å, c = 7.55 Å, and $\beta = 130^{\circ}$ [6]. In these crystals, the principal axis N_p is along the crystallographic b axis ([010]). N_m and N_g are in the a–c plane of the crystal.

Original Content from this work may be used under the terms of the Creative Commons Attribution 4.0 licence. Any further distribution of this work must maintain attribution to the author(s) and the title of the work, journal citation and DOI.

These crystals are particularly suitable for Tm doping because of their relatively broad emission band, large emission cross-section and low excited-state lifetime [7–15]. Based on the Hume–Rothery rule [16], stating the atomic radii, r_a , of the dopant and host atoms must differ by no more than 15%, Tm $(r_a = 175 \text{ pm})$ can substitute Y $(r_a = 180 \text{ pm})$ in KYW crystal. Thulium (Tm) doped crystals are used for developing nearinfrared (NIR) lasers [17], sensors [18], and on-chip quantum devices [19, 20]. The large cross-relaxation in Tm-doped crystals enables them to achieve high luminescence yield (\sim 2) with small thermal loading. Also, the 800 nm laser transition in these crystals makes efficient pumping with a diode laser possible. Among different host crystals, Tm-doped potassium double tungstate crystals are considered for building versatile and high-power NIR lasers thanks to their broadband and efficient radiation [7–9, 17]. The change in optical properties of these crystals due to growth conditions [10] and ion concentration has been investigated, in order to characterize their effect on these cross-relaxation processes. Understanding ionion interactions at high concentration is important for developing efficient lasing [17] or light storage [21, 22].

^{*} Author to whom any correspondence should be addressed.

An excess concentration of rare-earth ions, in part, induces strong magnetic and/or electric dipole–dipole interactions between neighboring ions. As a result, the ions experience enhanced cross-relaxation or quenching effects. The enhancement of nonradiative decay in high atomic density rare-earth crystals has been observed [23], while instantaneous spectral diffusion and excitation-induced decoherence have been extensively studied in various rare-earth doped systems [24–27].

The spectroscopic properties of a Tm³⁺-doped KYW crystal at room temperature have been studied for lasing applications [11, 12], however the behavior of cross-relaxation processes [28] in Tm: KYW at low temperatures remains unexplored. At these reduced temperatures, thermally induced nonradioactive processes become negligible and inhomogeneous broadening is reduced, offering a clearer understanding of cross-relaxation phenomena. Furthermore, measuring the ground-state population lifetime via spectral hole burning becomes feasible, with the hole's area offering additional insights into the process. Here, we investigate the properties of densely doped Tm in potassium yttrium double tungstate crystals. We report our experimental studies of Tm³⁺-doped KYW crystal at 4 K temperature. We use resonant excitation to study photoluminescence at cryogenic temperatures and observe non-radiative decay near the center of inhomogeneously broadened atomic spectrum.

2. Experimental results and analysis

A 5% Tm³⁺-doped KYW crystal (obtained from Optogama manufactured via the Czochralski method) with dimensions $3 \times 4 \times 5$ mm (crystal axis $N_{\rm p}$, $N_{\rm m}$, $N_{\rm g}$) is mounted on the platform of a Montana Cryostat (Fusion) with a base temperature of 4 K. With this doping concentration, Tm³⁺ ions have an estimated distance of ~ 1 nm from each other. A permanent magnet with dimensions of $15 \times 15 \times 15$ mm (N52 magnet from K&J Magnetics) is placed near the crystal, producing a magnetic field of approximately 0.1 T in the center of the crystal parallel to the $N_{\rm p}$ axis. Tm³⁺ ion has a nuclear spin of $\frac{1}{2}$, and a magnetic field of 0.1 T will split its ground state into two energy levels separated by ~ 10 MHz. This additional energy level is needed to create permanent holes after pumping (spectral hole burning).

2.1. Absorption

We initially used a Ti: sapphire laser (M Squared Lasers) to measure the absorption spectrum when the laser pulse is vertically polarized ($E \parallel N_{\rm m}$). The large absorption bandwidth and the relatively small mode-hop-free scanning range of our laser makes it difficult to directly observe the absorption spectrum by scanning the laser wavelength between 780 nm and 820 nm. Moreover, the high optical density near the center of

the inhomogeneous broadening creates a flat absorption spectrum and limits the ability to measure CW absorption [29]. Instead, the pulse measurement and its saturation is used to extract both absorption strength and saturation time. Using the pulsed measurement, we then recorded absorption of light from a diode laser with wavelength in the range of 793.4 nm and 794.4 nm. A laser pulse with duration of 5 ms and power of 5 mW is sent through the crystal with $E \parallel N_p$ (N_p is parallel to the crystallographic b axis). One example of the pulse's transmission intensity is shown in figure 1(a). The transmission intensity versus time is fitted with an exponential equation I(t) = a * (1 - exp(-t/b)) + c, where c is an offset constant, a/(a+c) is the absorption contrast and b is the saturation time [30]. By controlling the laser diode temperature (3 °C–48 °C), we can tune the output laser frequency of the Toptica laser (Model: DFB Pro laser head). We extract the absorption contrast and saturation time from the transmission intensity of the pulse, while varying the wavelength of the probe. Due to high doping concentration of Tm³⁺ ions, the crystal absorption at wavelengths between 793.65 nm and 794.1 nm, where atomic density is largest, is strong. In this region of the spectrum, the saturation effect could not be observed and transmission is near zero at typical pump powers used. We model the nonradiative behaviors of Tm³⁺ ions around the center of its inhomogeneous broadening, where excited ions are close enough to induce nonradiative decay, shown in figure 1(b). As we can see from the figure, the radiative decay intensity decreases while saturation time increases when pump wavelength approaches the center of the inhomogeneous broadening spectrum (where atomic density is higher). We use the Inokuti-Hirayama model [15, 31], which assumes an excited Tm³⁺ ion nonradiatively transfers its energy to the neighboring ions in the ground state. The photon intensity of the decay with respect to time follows the function:

$$I(t) = I_0 \exp\left(-\frac{t}{T_0} - \Gamma\left(1 - \frac{3}{s}\right) \frac{N}{c_o} \left(\frac{t}{T_0}\right)^{3/s}\right)$$
 (1)

where T_0 is the intrinsic lifetime of an isolated Tm^{3+} ion, c_0 is the critical ion concentration where nonradiative energy transfer emerges, N/c_0 is the concentration of atoms relative to the critical density for nonradiative transfer, and $\Gamma(x)$ is the Euler gamma function at the value of x. The parameter s characterizes the form of ion–ion interactions, in which dipole–dipole, dipole–quadrupole or quadrupole–quadrupole interactions correspond to s=6,8, or 10 respectively. The expected modulation of the radiative intensity due to this exchange is given by

$$\phi(\Delta, t) = \exp\left(-\frac{\Delta^2}{2\sigma^2}\right)$$

$$\times \exp\left(-\Gamma\left(1 - \frac{3}{s}\right) \frac{N(\Delta)}{c_0} \left(\frac{t}{T_0}\right)^{3/s}\right)$$
 (2)

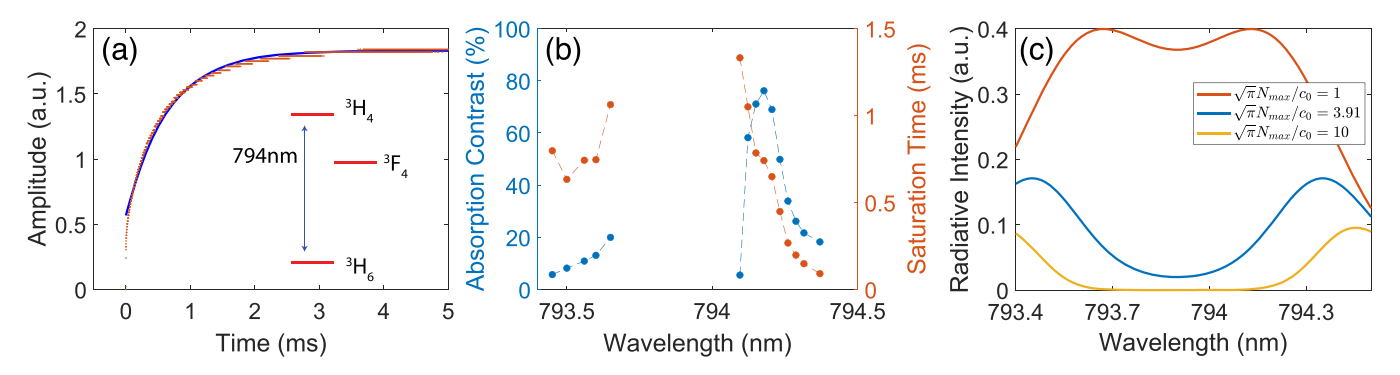


Figure 1. Absorption spectrum of thulium ions around 794 nm. (a) Measured transmission intensity of a 5 ms laser pulse passing through the crystal at a fixed wavelength (λ =794.205 nm). An exponential curve is fitted to the experimental data. The observed saturation is used to measure the strength of absorption (from absorption contrast) at different wavelengths. (b) Measured absorption contrast and saturation time with different wavelengths. Error bars are smaller than the data points. (c) Analytical modeling for varying frequency and emitter concentration shows suppression of absorption near resonance due to non-radiative decay processes considered in the model. The difference between the plotted wavelength in (b) and (c), and the center absorption wavelength of the broadened ensemble is proportional to Δ in equation (2).

where Δ is the detuning from resonance of the broadened ensemble and σ is the standard deviation of the inhomogeneous broadening. Equation (2) is plotted in figure 1(c) for varying frequency and emitter concentration. The behavior of $N(\Delta)/c_0$ is found from the experimental fitting later described in figure 2(b); these experimental values are plotted as the blue curve. Changing the concentration of emitters in the crystal results in a suppression or enhancement of this effect, as shown in the red and yellow curves respectively. The simulation results also well explain the observed phenomenon that photon transmission are very weak and the saturation time is extended when the wavelength approaches the center of the inhomogeneous broadening, where ion density is highest. Near the center of the spectrum ($\lambda = 793.7-794.1$ nm), light is fully absorbed and no contrast or saturation can be observed.

2.2. Excited state decay

Photoluminescence measurements are taken for ${}^3H_4 \leftrightarrow {}^3H_6$ at a pump wavelength between 794.05 nm and 794.55 nm with a single photon detector (from Laser Components) operating around 800 nm, which will only capture the decay behavior of ${}^3H_4 \leftrightarrow {}^3H_6$, since atoms undergoing other decay paths will emit photons at different wavelengths. Simple exponential fittings of the decay curves give the PL lifetimes, shown in figure 2(a). When the wavelength is closer to center of the inhomogeneous broadening, the PL lifetime becomes shorter and the simple exponential fitting becomes less accurate. In these scenarios, the nonradiative decay reduces the optical lifetime and leads to a nonexponential PL decay [32]. We refer to equation (1) and plot the decay curve as $ln[I(t)/I_0] + t/T_0$ versus $t^{3/6}$, shown in the inset figure of figure 2(b).

Two-pulse echo experiments were conducted with pulses as short as $0.1~\mu s$ to measure the optical coherence time. The maximum optical power used was 15 mW with beam size of about 0.07~mm inside the crystal. However, the echo signal was not detectable. We believe that the coherence time is too short (in the order between 1ns and 10~ns) to observe an echo within the timing resolution of our measurement devices.

When finding the inhomogeneous linewidth, the total absorption in the center of the line makes it difficult to fit the exact Gaussian distribution. We thus choose to place the center of the inhomogeneous distribution at the center of the region of complete absorption in figure 1(b), 739.9 nm. With our mean set, we can use the remaining points to fit the linewidth of the inhomogeneous distribution to 0.552 nm, or 300 GHz. The calculated broadening of the material is similar to that of Lithium Niobate at low temperature and low concentration, or YLuAG at similar concentration [4], and we observe an approximately four-fold reduction in linewidth compared to room-temperature measurements [10]. The distribution shown in figure 2(b) is then used in equation (4) to provide the fitting for the ³H₄ lifetime in figure 3(a).

2.3. Decay paths and spectral hole burning

There are two decay paths for Tm³⁺ ions in the excited state ³H₄. They can directly decay to the ground state ³H₆, or decay to the intermediate level ³F₄ before decaying back to the ground state ³H₆. We use a single photon detector (from Micro Photon Devices) with large spectral bandwidth (800 nm–1700 nm) to capture both decay behaviors. We fit the PL signal with the following double exponential function, which gives a fast decay lifetime and a slow decay lifetime respectively, shown in figure 3(a),

$$f(t) = e^{-t/T_{\rm f}} + \frac{\beta}{2} \frac{T_{\rm s}}{T_{\rm s} - T_{\rm f}} \left(e^{-t/T_{\rm s}} - e^{-t/T_{\rm f}} \right). \tag{3}$$

Here, β is the branching ratio to the intermediate level ${}^{3}F_{4}$, T_{f} and T_{s} are the fast and slow decay lifetimes respectively [29]. The ${}^{3}H_{4}$ lifetime is then fit to an effective lifetime including cross-relaxation effects,

$$T'(\Delta) = \frac{T_0}{1 + \sqrt{\pi \frac{t}{T_0}} \frac{N(\Delta)}{c_0}} \tag{4}$$

where t, the time of observation, is taken to be a fitting parameter corresponding to the period where ${}^{3}\text{H}_{4} - {}^{3}\text{H}_{6}$ emissions

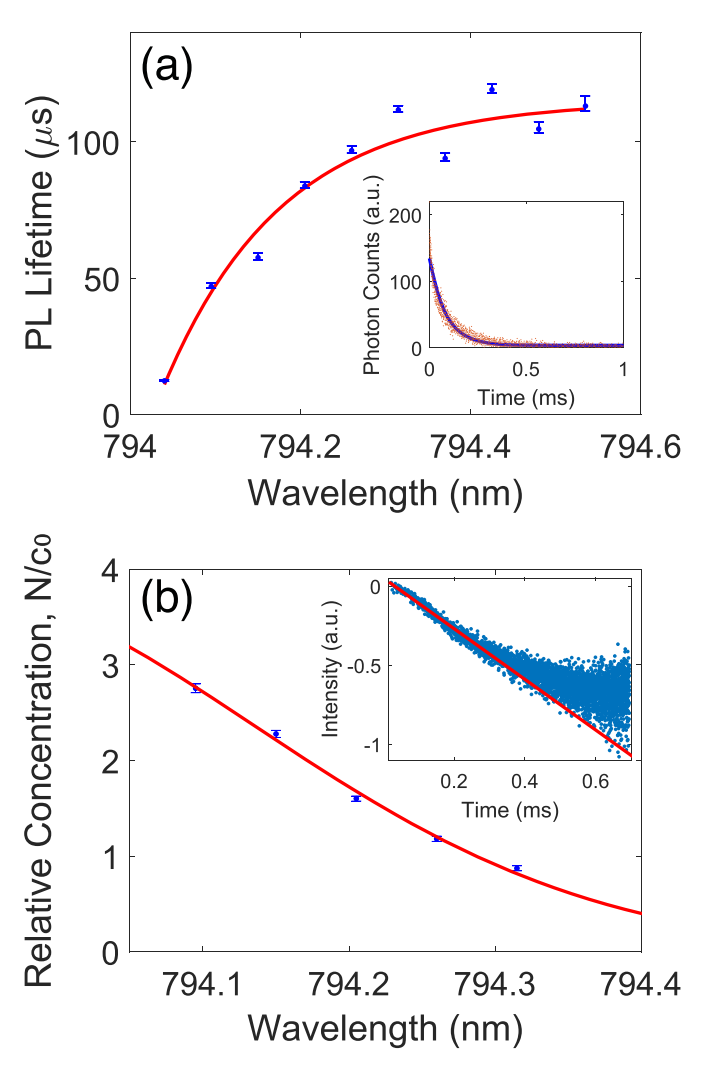


Figure 2. (a) Measurements of photoluminescence lifetime of the excited state 3H_4 as a function of pump wavelength. An exponential curve is fitted to guide the eye. The inset figure is the single-photon counts of spontaneous emissions at a wavelength of 794.205 nm, and a simple exponential decay curve is fitted to the data. (b) Extracted values for the relative transfer concentration found by fitting the intensity data to the Inokuti–Hirayama model, $\ln(I(t)/I(0)) + t/T_0$ versus \sqrt{t} . The red fit curve is a Gaussian centered at 793.9 nm with a linewidth of 0.552 nm, and the inset figure is the photoluminescence intensity at an arbitrary wavelength of 794.205 nm.

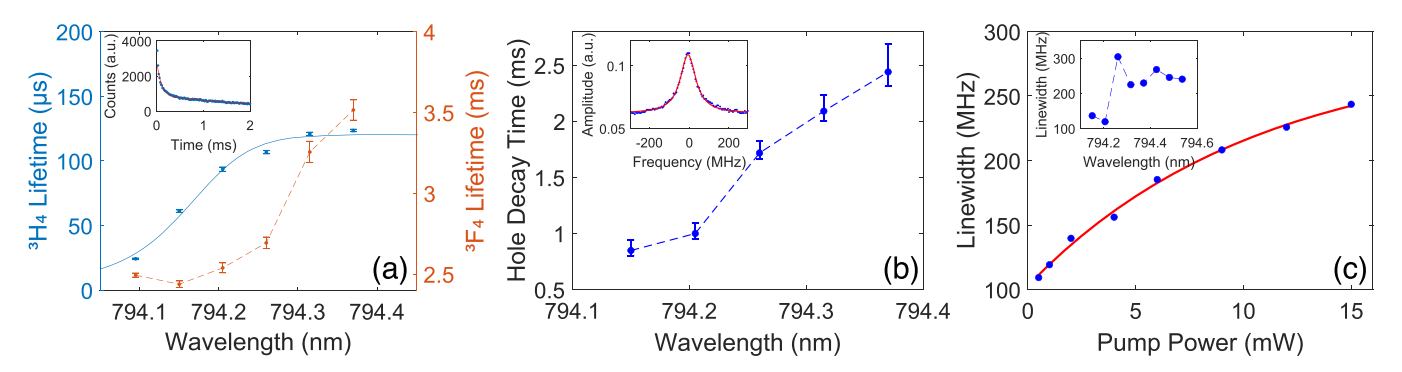


Figure 3. (a) Lifetime of the excited state 3H_4 and the intermediate state 3F_4 , obtained from a double exponential fit of the spontaneous emission data. The inset figure is the single-photon counts of the spontaneous emission at a pump wavelength of 794.205 nm, which consists of one fast decay and one slow decay. (b) Measurements of the spectral hole decay time with respect to different wavelengths. The inset figure is an example of spectral hole with Lorentzian fitting at a pump wavelength of 794.205 nm. (c) Measurement of spectral hole linewidth with respect to different pumping powers at a fixed wavelength ($\lambda = 794.205$ nm). The inset figure is the measurements of spectral hole linewidth with respect to different wavelengths. Error bars are much smaller than the data points.

Table 1. List of previous studies of P	L lifetime of Tm ³⁺ ion energ	y levels ³ F ₄ and	³ H ₄ in KX(WO ₄) ₂ cryst	als. Room temperature (RT) is
300 K.				

Crystal	Optical transition	Temperature	PL lifetime
Tm^{3+} : KY(WO ₄) ₂	$^{3}\text{F}_{4} \leftrightarrow ^{3}\text{H}_{6}$	RT	1.11–1.35 ms [11]
Tm^{3+} : $KY(WO_4)_2$	$^{3}\text{F}_{4} \leftrightarrow ^{3}\text{H}_{6}$	RT	1.34 ms [10]
Tm^{3+} , Ho^{3+} : $KY(WO_4)_2$	$^{3}\text{F}_{4} \leftrightarrow ^{3}\text{H}_{6}$	RT	1.8 ms [12]
Tm^{3+} : $KGd(WO_4)_2$	$^{3}\text{F}_{4} \leftrightarrow ^{3}\text{H}_{6}$	RT	1.76 ms [33]
Tm^{3+} : $KLu(WO_4)_2$	$^{3}\text{F}_{4} \leftrightarrow ^{3}\text{H}_{6}$	RT	0.9–1.34 ms [34]
Tm^{3+} : $KLu(WO_4)_2$	${}^{3}\mathrm{F}_{4} \leftrightarrow {}^{3}\mathrm{H}_{6}$	RT	1.48 ms [15]
	$^{3}\mathrm{H}_{4}^{3}\mathrm{H}_{6}$	RT	20–230 μs [15]
Tm^{3+} : $KYb(WO_4)_2$	${}^{3}\mathrm{F}_{4} \leftrightarrow {}^{3}\mathrm{H}_{6}$	RT	199–278 μs [35]
	$^{3}\mathrm{H}_{4}^{3}\mathrm{H}_{6}$	RT	9–90 μs [35]
Tm^{3+} : $KY(WO_4)_2$	$^{3}\text{F}_{4} \leftrightarrow ^{3}\text{H}_{6}$	4 K	2.5–3.5 ms [this study]
	${}^3F_4 \leftrightarrow {}^3H_6$	4 K	12–113 μ s [this study]

dominate the observed photoluminescence. We compare our lifetime measurements with the previous studies performed at room temperatures in table 1.

Pumping atoms at a fixed wavelength creates spectral holes as is expected from the saturation seen in figure 1(a). To reliably measure the decay time of the spectral hole, we use a series of short and weak pulses after the hole burning pulse and record their peak intensity over time. After sending a 10 ms pump pulse with a power of 5 mW, weak probe pulses are sent to the crystal every 50 μ s. The peak intensity of these pulses decays over time, indicating higher absorption as the spectral hole decays. The pulse duration and intensity is chosen such that its effect on the spectral hole is negligible. The decay of the intensity (increased absorption) is fitted with a single exponential to obtain the hole lifetime shown in figure 3(b). We observed that the hole decay lifetime is shorter than the PL lifetime of the slow decay, and we attribute this to the radiation trapping during PL due to the high atomic densities [36]. To investigate the effect on spectral hole linewidth, firstly a 10 ms pump pulse is sent to the crystal, followed by a weak probe pulse with its frequency being scanned by approximately 2 GHz in 100 μ s (via electrical modulation of the Toptica laser diode). By using a Lorentz fitting, we extract the linewidth of the spectral hole. To further understand the power broadening effect, we send pump pulses with different powers ranging from 0.5 mW to 15 mW. Based on our experimental observations on the coherence time of doped ions in previous experiments, laser pulse of 15 mW power with 10 ms duration will only cause negligible heating effects to the crystal. Only when the laser power goes above 15 mW with pulse duration longer than 100 ms, notable heating effects could be observed. The hole linewidths for different pump powers are shown in figure 3(c). We use the rate equation model for instantaneous spectral diffusion to fit the curve [24]:

$$\Gamma = \Gamma_{(P=0)} + \frac{1}{2} \Gamma_{\text{ISD}} \left(1 - e^{-c_{p}P} \right),$$
 (5)

where $\Gamma_{(P=0)}$ is the spectral linewidth at zero pump power, $\Gamma_{\rm ISD}$ represents ISD spectral broadening of full width

at half maximum, and c_p is a constant parameter with respect to excitation power, which depends on the ion–ion interaction strength. In the fitting of our data, we found $\Gamma_{(P=0)}=102.8(94.61,110.9)$ MHz and $\Gamma_{\rm ISD}=367.7(293.5,441.9)$ MHz, shown in figure 3(c). The hole linewidth appears to drop for pumping wavelength near the center of the inhomogeneously broadened atomic spectrum (see inset of figure 3(c)). We attribute this to stronger absorption and thus smaller power broadening near the center of the spectrum.

The magnetic field created by the permanent magnet will split the energy levels ${}^{3}H_{4}$ and ${}^{3}H_{6}$ by around 10 MHz. During the experiments, we could not observe two spectral holes. This is a result of the spectral broadening being much larger than the energy level splittings for our magnetic field.

3. Discussion and conclusions

We have investigated the spectral properties of a KY(WO₄)₂ crystal with 5% concentration of Tm³⁺ ions. By tuning the probe light frequency from the center of the inhomogeneous broadening, the effective optical density can be controlled. Close to the center of the inhomogeneously broadened atomic spectrum, the high atomic density of Tm ions in the KYW crystal leads to a strong non-radiative decay. These nonradiative transitions shorten the excited state lifetime by more than ten fold. As the optical density increases near resonance, i.e. increase in the effective ion density, the nonradiative energy transfer becomes more prominent due to the stronger ion-ion interactions, and this behavior is well explained by our theoretical model. We also investigated spectral properties of the intermediate excited level ³F₄ and observed that it can serve as a shelving level for spectral tailoring. In addition, the spectral hole lifetime is also observed to reduce by more than a factor of two as we approach the center of the inhomogeneous broadening. The lack of observation of two-pulse photon echo suggests that the high concentration of ions causes large spectral diffusion, which greatly increases the homogeneous linewidth.

J. Opt. **26** (2024) 095401

Data availability statement

All data that support the findings of this study are included within the article (and any supplementary files).

Acknowledgments

We acknowledge the support from U.S. Department of Energy, Office of Science, Office of Advanced Scientific Computing Research, through the Quantum Internet to Accelerate Scientific Discovery Program under Field Work Proposal 3ERKJ381.

Conflicts of interest

The authors declare no conflicts of interest.

ORCID iDs

Yisheng Lei https://orcid.org/0009-0004-1014-1189
Trevor Kling https://orcid.org/0000-0003-1496-7717
Mahdi Hosseini https://orcid.org/0000-0003-3109-6650

References

- [1] Sellin P, Strickland N, Carlsten J and Cone R 1999 Programmable frequency reference for subkilohertz laser stabilization by use of persistent spectral hole burning *Opt. Lett.* 24 1038
- [2] Kippenberg T, Kalkman J, Polman A and Vahala K 2006 Demonstration of an erbium-doped microdisk laser on a silicon chip *Phys. Rev.* A 74 051802
- [3] Luo Q *et al* 2023 On-chip erbium—ytterbium-co-doped lithium niobate microdisk laser with an ultralow threshold *Opt. Lett.* **48** 3447
- [4] Thiel C W, Böttger T and Cone R 2011 Rare-earth-doped materials for applications in quantum information storage and signal processing *J. Lumin.* 131 353
- [5] Lei Y, Asadi F K, Zhong T, Kuzmich A, Simon C and Hosseini M 2023 Quantum optical memory for entanglement distribution *Optica* 10 1511
- [6] Gallucci E, Goutaudier C, Boulon G, Cohen-Adad M T and Mentzen B 2000 Nonstoichiometric KY(WO₄)₂: crystal growth, chemical and physical characterization *J. Cryst. Growth* 209 895
- [7] Gaponenko M, Onushchenko A, Kisel V, Malyarevich A, Yumashev K and Kuleshov N 2012 Compact passively Q-switched diode-pumped Tm:KY(WO₄)₂ laser with 8 ns/30 µj pulses Laser Phys. Lett. 9 291
- [8] Lagatsky A, Calvez S, Gupta J, Kisel V, Kuleshov N, Brown C, Dawson M and Sibbett W 2011 Broadly tunable femtosecond mode-locking in a Tm:KYW laser near 2 μm Opt. Express 19 9995
- [9] Gaponenko M, Loiko P, Gusakova N, Yumashev K, Kuleshov N and Pavlyuk A 2012 Thermal lensing and microchip laser performance of N_g-cut Tm³⁺:KY(WO₄)₂ crystal Appl. Phys. B 108 603
- [10] Guretskii S *et al* 2021 Tm³⁺:KY(WO₄)₂ single crystals: controlled growth and spectroscopic assessment *Opt. Mater.* 120 11145]
- [11] Troshin A, Kisel V, Yasukevich A, Kuleshov N, Pavlyuk A, Dunina E and Kornienko A 2007 Spectroscopy and laser

- properties of Tm³⁺:KY(WO₄)₂ crystal *Appl. Phys.* B **86** 287
- [12] Lagatsky A, Fusari F, Kurilchik S, Kisel V, Yasukevich A, Kuleshov N, Pavlyuk A, Brown C and Sibbett W 2009 Optical spectroscopy and efficient continuous-wave operation near 2 μm for a TM, HO:KYW laser crystal Appl. Phys. B 97 321
- [13] Mateos X, Solé R, Gavalda J, Aguiló M, Massons J and Díaz F 2006 Crystal growth, optical and spectroscopic characterisation of monoclinic KY(WO₄)₂ co-doped with Er³⁺ and Yb³⁺ Opt. Mater. 28 423
- [14] Kumaran A S, Chandru A L, Babu S M and Ichimura M 2005 Growth and characterization of pure and doped KY(WO₄)₂ crystals J. Cryst. Growth 275 e1901
- [15] Silvestre O, Pujol M C, Rico M, Güell F, Aguiló M and Díaz F 2007 Thulium doped monoclinic KLu(WO₄)₂ single crystals: growth and spectroscopy Appl. Phys. B 87 707
- [16] Egami T and Waseda Y 1984 Atomic size effect on the formability of metallic glasses J. Non-Cryst. Solids 64 113
- [17] Gaponenko M, Kuleshov N and Südmeyer T 2014 Efficient diode-pumped Tm:KYW 1.9-\mu microchip laser with 1 W cw output power Opt. Express 22 11578
- [18] Shen Y, Zhao W, He J, Sun T and Grattan K T V 2003 Fluorescence decay characteristic of Tm-doped YAG crystal fiber for sensor applications, investigated from room temperature to 1400°C *IEEE Sens. J.* **3** 507
- [19] Pak D, Nandi A, Titze M, Bielejec E S, Alaeian H and Hosseini M 2022 Long-range cooperative resonances in rare-earth ion arrays inside photonic resonators *Commun. Phys.* 5 89
- [20] Dutta S, Zhao Y, Saha U, Farfurnik D, Goldschmidt E A and Waks E 2023 An atomic frequency comb memory in rare-earth-doped thin-film lithium niobate ACS Photonics 10 1104
- [21] Gorshkov A V, André A, Fleischhauer M, Sørensen A S and Lukin M D 2007 Universal approach to optimal photon storage in atomic media *Phys. Rev. Lett.* 98 123601
- [22] Saglamyurek E, Jin J, Verma V B, Shaw M D, Marsili F, Nam S W, Oblak D and Tittel W 2015 Quantum storage of entangled telecom-wavelength photons in an erbium-doped optical fibre *Nat. Photon.* 9 83
- [23] Kustov E, Loschenov V and Basieva I 2014 Decay times of radiative and non-radiative transitions in rare-earth ions *Phys. Scr.* 2014 014032
- [24] Thiel C, Macfarlane R, Sun Y, Böttger T, Sinclair N, Tittel W and Cone R 2014 Measuring and analyzing excitation-induced decoherence in rare-earth-doped optical materials *Laser Phys.* 24 106002
- [25] Ahlefeldt R, McAuslan D, Longdell J, Manson N and Sellars M 2013 Precision measurement of electronic ion-ion interactions between neighboring Eu³⁺ optical centers *Phys. Rev. Lett.* 111 240501
- [26] Rančić M et al 2022 Electron-spin spectral diffusion in an erbium doped crystal at millikelvin temperatures Phys. Rev. B 106 144412
- [27] Louchet-Chauvet A and Chanelière T 2023 Strain-mediated ion-ion interaction in rare-earth-doped solids J. Phys.: Condens. Matter 35 305501
- [28] Fan T Y, Huber G, Byer R L and Mitzscherlich P 1988 Spectroscopy and diode laser-pumped operation of Tm,Ho:YAG IEEE J. Quantum Electron. 24 924
- [29] Sinclair N, Oblak D, Saglamyurek E, Cone R L, Thiel C W and Tittel W 2021 Optical coherence and energy-level properties of a Tm3⁺-doped LiNbO₃ waveguide at subkelvin temperatures *Phys. Rev.* B 103 134105
- [30] Yang L, Lin H, Feng X, Plimmer M and Zhang J 2019 Saturation cavity ring-down spectrometry using a dynamical relaxation model Opt. Express 27 1769

- [31] Inokuti M and Hirayama F 1965 Influence of energy transfer by the exchange mechanism on donor luminescence *J. Chem. Phys.* **43** 1978
- [32] Scarafagio M *et al* 2019 Ultrathin Eu-and Er-doped Y₂O₃ films with optimized optical properties for quantum technologies *J. Phys. Chem.* C **123** 13354
- [33] Güell F, Gavaldà J, Solé R, Aguiló M, Diaz F, Galan M and Massons J 2004 1.48 and 1.84 μ m thulium emissions in monoclinic KGd(WO₄)₂ single crystals *J. Appl. Phys.* 95 919
- [34] Petrov V, Cinta Pujol M, Mateos X, Silvestre Ò, Rivier S, Aguilo M, Solé R M, Liu J, Griebner U and Diaz F 2007

- Growth and properties of KLu(WO₄)₂ and novel ytterbium and thulium lasers based on this monoclinic crystalline host *Laser Photonics Rev.* **1** 179
- [35] Pujol M, Güell F, Mateos X, Gavalda J, Solé R, Massons J, Aguiló M, Díaz F, Boulon G and Brenier A 2002 Crystal growth and spectroscopic characterization of Tm³⁺ -doped KYb(WO₄)₂ single crystals *Phys. Rev.* B 66 144304
- [36] Sumida D and Fan T 1994 Effect of radiation trapping on fluorescence lifetime and emission cross section measurements in solid-state laser media *Opt. Lett.* 19 1343